Direct Observation of a Hydrogen Atom Adduct to C-5 in Uracil. A Neutralization-Reionization Mass Spectrometric and ab Initio Study

Erik A. Syrstad, Shetty Vivekananda, and František Tureček*

Department of Chemistry, Bagley Hall, Box 351700, University of Washington, Seattle, Washington 98195-1700

Received: April 10, 2001; In Final Form: July 2, 2001

The elusive hydrogen atom adduct to the C-5 position in uracil was generated specifically in the gas phase, and its unimolecular dissociations were elucidated by neutralization−reionization mass spectrometry. Collisional electron transfer to the 5,6-dihydrouracil-6-yl cation generated the 5,6-dihydropyrimidine-2,4(*1H,3H*)-dion-6-yl radical (**1**), which was the most stable hydrogen atom adduct to C-5 in uracil. A substantial fraction of **1** was stable on the 5.1 μs time scale. The main unimolecular dissociations of **1** were specific losses of hydrogen atoms from C-5 and ring cleavages, as determined by deuterium labeling. Radical **1** did not isomerize unimolecularly to 5,6-dihydropyrimidine-2,4(*1H,3H*)-dion-5-yl (**2**). Ab initio calculations up to effective QCISD(T)/6-311+G(3df,2p) and combined density functional theory and perturbational calculations up to B3-MP2/6-311+G(3df,2p) provided bond dissociation and transition state energies for several radical and ion dissociations that were used for assessing rate constants by RRKM theory. The observed dissociations occur to a large part from excited electronic states of uracil radicals that are formed by vertical electron capture. The adiabatic ionization energies of uracil and **1** were calculated as 9.24 and 6.70 eV, respectively.

Introduction

Nucleobase residues in DNA and RNA are susceptible to attack by energetic particles produced by radiation or chemical processes.[1] In particular, radiolysis of water produces electrons and small radicals (H, OH, etc.) that are known to add to the nucleobases and cause chemical modifications that are referred to as radiation damage.[1,2] Although the kinetics of radical additions to the four DNA nucleobases have been studied in detail, much less is known about the reactivity of the RNA nucleobase uracil. Flossman, Westhof, and co-workers studied the formation of uracil radicals following irradiation with 100 kV X-rays[3] or upon photosensitized irradiation with UV light.[4] Electron paramagnetic resonance spectra indicated the formation of several transient species that were assigned to hydrogen atom adducts to uracil. Von Sonntag and co-workers studied pulse radiolysis of uracil derivatives in aqueous solution and concluded that hydrogen atom adducts to O-4 and C-6 were formed by protonation of the intermediate uracil anion radical.[5] For the ring numbering in uracil, see the formulas below. Two mechanisms for the formation of hydrogen atom adducts to nucleobases have been suggested, as shown for uracil in Scheme 1.[1] The first mechanism (mechanism I) assumes direct addition to the nucleobase of a hydrogen atom produced by radiolysis of water. The presumed sites of H atom additions are at the C-5−C-6 double bond to produce radicals **1** or **2**.[6] Mechanism I is analogous to that presumed for the addition of OH radicals to nucleobases;[7] however, additions of H atoms are much less thoroughly documented.[1,2] The second mechanism (mechanism II) presumes addition of a thermal electron to form a uracil anion-radical. The latter is protonated by the solvent or an acid present in the solution to give the H atom adduct **3**.[8]

Although the radiation chemistry of uracil and other pyrimidine nucleobases has been studied extensively, most of the results obtained so far provided only indirect evidence of the existence of transient radicals through redox reactions[2] and UV−vis absorption spectra.[9] Under radiolytic or photolytic conditions, a variety of products are typically formed that are monitored spectroscopically in the mixture.[5,9,10] Structures and intrinsic properties of nucleobase radicals are therefore not amenable to analysis. Limited information about the structures and energetics of several nucleobase radicals has been provided by ab initio calculations that were carried out at low[6] to medium levels of theory.[11]

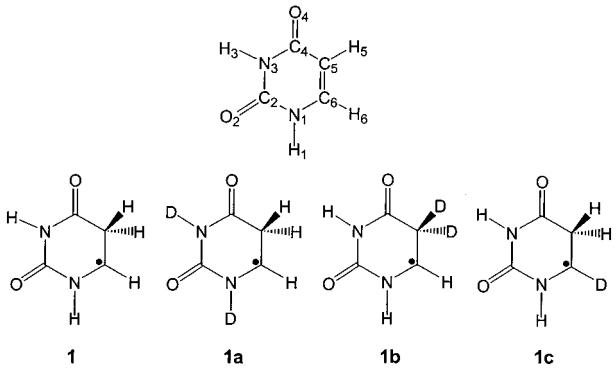

SCHEME 1

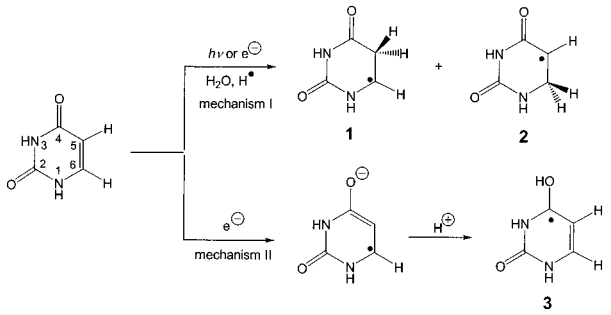

* To whom correspondence should be addressed. Tel.: (206) 685-2041. Fax: (206) 685-3478. E-mail: turecek@chem.washington.edu.

10.1021/jp011349r CCC: $20.00
Published on Web 08/16/2001

We now describe the targeted, specific preparation of two pivotal uracil radicals relevant to radiolytic mechanisms I and II.[12] In the present paper, we report on the specific formation in the gas phase of 5,6-dihydropyrimidine-2,4(*1H,3H*)-dion-6-yl (**1**), which is the elusive intermediate of H atom addition to C-5 in uracil. We prepared radical **1** by femtosecond collisional electron transfer to its cationic precursor $\mathbf{1}^+$, and studied the mechanisms of radical unimolecular dissociations by neutralization-reionization mass spectrometry[13,14] with the help of deuterium-labeled derivatives **1a**−**1c**. In addition, we report detailed ab initio calculations, performed at high levels of theory, up to effective QCISD(T)/6-311+G(3df,2p), of radical **1**, several of its isomers, dissociation products, and relevant transition states. Excited electronic states are found to play an important role in the unimolecular chemistry of **1** and are therefore addressed by time-dependent density functional theory calculations.[15] In an accompanying paper, we address the chemistry of 4-hydroxy-3,4-dihydropyrimidine-2(*1H*)-on-4-yl radical (**3**), which is the elusive intermediate of protonation at O-4 in uracil anion-radical.[16]

Experimental Part

Materials. Uracil, 2-pentenoic acid, urea, and ethyl-3-oxopentanoate (all Aldrich) were used as received. Deuterium-labeled reagents, sodium borodeuteride (99% D, Aldrich), ND_3 (Matheson, 99% D), D_2O, CD_3OD, and acetone-d_6 (all Cambridge Isotope Laboratories) were also used as received. 6-Ethyl-5,6-dihydropyrimidine-2,4(*1H,3H*)-dione (**4**) was synthesized according to literature,[17] and recrystallized from water, yield 27%, mp 194 °C. ^{1}H NMR (300 MHz, $CDCl_3$): 1.0 (t, 3H, $-CH_2C\mathbf{H}_3$), 1.64 (m, 2H, $-C\mathbf{H}_2CH_3$), 2.42 (dd, 1H, H-5), 2.70 (dd, 1H, H-5), 3.55 (m, 1H, H-6), 5.60 (broad s, 1H, N−H), 7.62 (broad s, 1H, N−H). 70 eV mass spectrum (*m*/*z*, rel intensity): 142 (9), 114 (5), 113 (100), 112 (35), 71 (3), 70 (80), 58 (3), 56 (7), 43 (23), 42 (7), 41 (7).

6-Ethyl-5,6-dihydropyrimidine-2,4(*1D,3D*)-dione (4a). Compound **4** (144 mg, 1 mmol) was dissolved in THF (13 mL) and stirred overnight at 20 °C. Then, 11 mL of CH_3OD was added and the solution was stirred for 10 min, followed by solvent evaporation under vacuum at room temperature. 70 eV mass spectrum of **4a** was (*m*/*z*, rel intensity) 145 (2), 144 (11), 143 (7), 142 (2), 116 (5), 115 (80), 114 (76), 113 (26), 112 (4), 72 (5), 71 (100), 70 (29), 59 (6), 58 (8), 57 (13), 56 (7), 55 (7).

6-Ethyl-5,6-dihydro-5,5-d_2-pyrimidine-2,4(*1H,3H*)-dione (4b). Compound **4** (160 mg, 1.1 mmol) was dissolved in 43 mL D_2O containing 450 mg K_2CO_3. The solution was stirred 72 h at 20 °C, acidified with 37% DCl in D_2O, and solvent was evaporated to dryness in vacuo. The product was taken in methanol, the solution was filtered, and the solvent was evaporated in vacuo. 70 eV mass spectrum (*m*/*z*, rel intensity): 148 (4), 147 (3), 146 (3), 145 (4), 144 (9), 143 (1), 116 (14), 115 (100), 114 (11), 113 (31), 73 (8), 72 (86), 71 (8).

6-Ethyl-6-*d*-5,6-dihydropyrimidine-2,4(*1H,3H*)-dione (4c) was prepared from ethyl 3-oxopentanoate in five steps, as follows.

Ethyl 3-hydroxypentanoate-3-*d* (5). Ethyl 3-oxopentanoate (5.0 g, 34.7 mmol) was dissolved in 25 mL of methanol and added at 0 °C to a solution of sodium borodeuteride (0.73 g, 16.6 mmol) in methanol (25 mL). The mixture was stirred at 0 °C for 45 min, acidified with acetic acid (2 g), and the solvent was evaporated in vacuo. The residue was extracted with ether (4 × 25 mL), dried, and the solvent was evaporated in vacuo to yield 4.9 g (96%) of an oily product. GC-MS showed essentially one peak corresponding to **5** (*m*/*z* 118, 102, 90, 88, 84, 76, 72, 60, 57), and a small amount (<5%) of a methyl ester (*m*/*z* 104, 74, 72, 62, 60, 59, 57).

Ethyl 3-(*p*-toluenesulfonyloxy)pentanoate-3-*d* (6) was prepared by tosylation of ester **5** (*p*-toluenesulfonyl chloride, pyridine, 0 °C, 48 h) followed by standard workup (ice water, extraction with chloroform, drying with $MgSO_4$ followed by solvent evaporation). Crude tosylate **6** was used further without purification.

Ethyl 2-pentenoate-3-*d* (7). Crude tosylate **6** (34 mmol) was dissolved in tetrahydrofuran (40 mL), cooled to −78 °C, and potassium *t*-butoxide (3.8 g, 34 mmol) was added under nitrogen. The reaction mixture was stirred at −78 °C for 2 h and then allowed to warm to room temperature. Pentane (50 mL) was added, and the slurry was poured on ice/water (300 mL), the organic layer was separated, and the aqueous layer was extracted with 3 × 25 mL of pentane. The pentane solution was washed with brine, dried with magnesium sulfate and decolorized with active charcoal. Pentane was distilled off through a 20 cm Vigreux column, and the residue was distilled at ca. 100 Torr to yield 4.4 g of ester **7**. Mass spectrum: *m*/*z* 129 ($M^{+\bullet}$).

2-Pentenoic acid-3-*d* (8). Ethyl 2-pentenoate-3-*d* (**7**, 4.4 g, 34 mmol) was dissolved in a mixture of methanol (25 mL) and water (5 mL), sodium hydroxide (2.4 g, 60 mmol) was added and the solution was refluxed for 3 h. The solvents were evaporated and the residue was taken in water, acidified to pH 1 with hydrochloric acid, and extracted with five 25 mL portions of dichloromethane. Workup followed by distillation gave 2.45 g (71%) of **8**, bp 100 °C/20 Torr.

6-Ethyl-6-*d*-5,6-dihydropyrimidine-2,4(*1H,3H*)-dione (4c). 2-Pentenoic acid-3-*d* (**8**, 2.4 g, 24 mmol) and urea (3.65 g, 61 mmol) were heated in a stainless steel pressure vessel (40 mL volume) at 195 °C for 2 h.[17] The vessel was cooled to room temperature, depressurized to release ammonia, and the gummy residue was dissolved in 50 mL of warm water. The warm solution was decolorized with active charcoal, filtered, and the filtrate volume was reduced to 15 mL on a rotavap. Compound **4c** crystallized upon standing at 4 °C. The crystals were collected and recrystallized once from water. Yield 650 mg (19%), mp 192 °C. 70 eV mass spectrum (*m*/*z*, rel intensity): 144 (1), 143 (11), 142 (2), 115 (7), 114 (100), 113 (51), 112 (5), 72 (3), 71 (75), 70 (12), 60 (4), 59 (2), 57 (4), 56 (3), 44 (12), 43 (14), 42 (5), 41 (3). ^{1}H NMR (300 MHz, $CDCl_3$): 1.0 (t, 3H, $-CH_2C\mathbf{H}_3$), 1.62 (m, 2H, $-C\mathbf{H}_2CH_3$), 2.42 (d, 1H, H-5), 2.70 (d, 1H, H-5), 5.35 (broad s, 1H, N−H), 7.40 (broad s, 1H, N−H).

Methods

Measurements were carried out on a tandem quadrupole acceleration−deceleration mass spectrometer described previously.[18] Electron ionization was used to generate cations $\mathbf{1}^+$−$\mathbf{1c}^+$ in a standard electron ionization source. Typical ionization conditions were as follows: electron energy 70 eV, emission current 500 μA, temperature 200−250 °C. Ion−molecule reactions and charge exchange ionization were carried out in a tight chemical ionization (CI) source. Typical ionization conditions were as follows: electron energy 100 eV, emission current 1−2 mA, temperature 280−300 °C, ion source potential 80 V. NH_3, ND_3, acetone, CD_3COCD_3, and 2-methylpropane, water, and D_2O were used as CI reagent gases at pressures $1.0-1.5 \times 10^{-4}$ Torr as read on an ionization gauge located at the diffusion pump intake. Stable precursor ions were passed through a quadrupole mass filter operated in the radio frequency-only mode, accelerated to the total kinetic energy of 8250 eV and neutralized in the collision cell floated at −8170 V. The

precursor ion lifetimes were 30−40 μs. Dimethyl disulfide (DMDS) was admitted to the differentially pumped collision cell (cell I) at a pressure such as to achieve 70% transmittance of the precursor ion beam. The ions and neutrals were allowed to drift to a four segment conduit,[19] where the ions were reflected by the first segment floated at +250 V. The neutral flight times in standard NRMS measurements were 5.1 μs. The fast neutral species were reionized in a second cell (cell II) by collision with oxygen at a pressure adjusted such as to achieve 70% transmittance of the precursor ion beam. The ions formed in cell II were decelerated, energy filtered, and analyzed by a quadrupole mass filter operated at unit mass resolution. The instrument was tuned daily to maximize the ion current of reionized $CS_2^{+\bullet}$. Typically, 40 repetitive scans were accumulated per spectrum. Collisional activation of transient radicals (denoted as NCR) was carried out in the differentially pumped conduit between cell I and cell II using He at pressures to achieve 50% precursor beam transmittance. The conduit segments were maintained at +250 V to prevent detection of any reionized species formed in this region.

Collisionally activated dissociation (CAD) spectra were measured on a JEOL HX-110 double-focusing mass spectrometer of forward geometry (the electrostatic sector E precedes the magnet B). Ion collisions with air were monitored in the first field-free region at pressures to achieve 70% transmittance of the ion beam at 10 keV. The spectra were obtained by scanning E and B simultaneously while maintaining a constant B/E ratio (B/E linked scan).

Calculations

Standard ab initio and density functional theory calculations were performed using the Gaussian 98 suite of programs.[20] Geometries were optimized using Becke's hybrid functional (B3LYP)[21] and the 6-31+G(d,p) basis set. For some species, geometries were optimized with Hartree−Fock calculations, HF/6-31G(d,p) and HF/6-31+G(d,p), as specified below. Spin-unrestricted calculations (UB3LYP and UHF) were used for open-shell systems. Spin contamination in the UB3LYP calculations was small as judged from the $\langle S^2 \rangle$ operator expectation values that were 0.75−0.77. The optimized structures were characterized by harmonic frequency analysis as local minima (all frequencies real) or first-order saddle points (one imaginary frequency). Complete optimized structures in the Cartesian coordinate format and total energies are available from the correspondence author upon request. The B3LYP/6-31+G(d,p) frequencies were scaled by 0.963 (ref 22, for other scaling factors see ref 23), the UHF/6-31G(d,p) frequencies were scaled by 0.893, and used to calculate zero-point vibrational energies (ZPVE), enthalpy corrections, and partition functions. The rigid-rotor harmonic oscillator approximation was used in all thermochemical calculations. Single-point energies were calculated at several levels of theory. In three sets of calculations, MP2-(frozen core)[24] and B3LYP energies were calculated with basis sets of increasing size, e.g., 6-311+G(2d,p), 6-311+G(2df,p), and 6-311+G(3df,2p). Spin contamination in the UMP2 calculations was moderate for uracil radicals and transition states, as evidenced by the spin expectation values $\langle S^2 \rangle$ that ranged between 0.76 and 0.91. Spin annihilation using Schlegel's projection method[25] (PMP2)[20] reduced the $\langle S^2 \rangle$ values to 0.75−0.76. In addition, restricted open-shell (ROMP2) calculations[26] were carried out for the entire set of structures to deal with spin contamination.[27] The PMP2 and ROMP2 energies were averaged with the B3LYP energies according to the empirical procedure that was introduced previously[14a,14b,28] and tested for several systems since.[29,30] This resulted in error cancellation and provided relative energies denoted as B3−PMP2 or B3−ROMP2[30] as discussed below. Calculations on closed-shell systems are marked by B3-MP2. In addition, a composite procedure was adopted that consisted of a single-point quadratic configuration interaction calculation,[31] QCISD(T)/6-31G(d,p), and basis set expansion up to 6-311+G(3df,2p) through PMP2 or ROMP2 single-point calculations according to eq 1:

$$\text{QCISD(T)/6-311+G(3df,2p)} \approx \text{QCISD(T)/6-31G(d,p)} + \text{MP2/6-311+G(3df,2p)} - \text{MP2/6-31G(d,p)} \quad (1)$$

This level of theory is intermediate between those of the Gaussian 2 (MP2) method[32] which uses the 6-311G(d,p) basis set in the large QCISD(T) calculation and the G2(MP2, SVP) method[33] which uses the 6-31G(d) basis set instead. We also utilized the previous finding that restricted open-shell calculations (ROMP2) provided good stabilization energies for small organic radicals.[27] Basis set expansions to effective QCISD/6-311+G(2d,p), QCISD(T)/6-311+G(2d,p), and QCISD(T)/6-311+G(2df,p) were also tested for selected systems.

Franck−Condon energies in vertical neutralization and reionization were taken as absolute differences between the total B3-MP2/6-311+G(2d,p) energies of fully optimized ion or neutral structures and those in which an electron has been added to an optimized cation structure or subtracted from an optimized neutral structure. No zero-point corrections were applied to the calculated Franck−Condon energies.

Gradient optimizations of excited-state geometries were performed with spin-unrestricted configuration interaction singles (UCIS)[34] using the 6-31+G(d,p) basis set. Improved energies for excited states were obtained from UCIS and time-dependent density functional theory[15] single-point calculations using the B3LYP hybrid functional and the larger 6-311+G(2d,p) basis set.

RRKM calculations used Hase's program[35] that was recompiled for MS-DOS and run under Windows NT.[36] Vibrational state densities were obtained by direct count of quantum states in 2 kJ mol^{-1} steps for internal energies up to 80−120 kJ mol^{-1} above the threshold. The rotational states were treated adiabatically[37] and the microscopic rate constants, $k(E,J,K)$, were Boltzmann-averaged over the thermal distribution of rotational J and K states pertaining to the ion source temperature. Thermal rate constants were calculated using the standard transition state theory formulas.[38] The activation energies were taken from single-point calculations and the partition functions were calculated from the B3LYP/6-31+G(d,p) moments of inertia and scaled harmonic frequencies using the rigid rotor-harmonic oscillator approximation.

Results and Discussion

Specific generation of radicals by neutralization-reionization mass spectrometry in the gas-phase relies on fast collisional electron transfer to a cationic precursor. The precursor cation is synthesized by the methods of gas-phase chemistry, accelerated to a high velocity (118 625 m s^{-1} for $\mathbf{1}^+$) and discharged by a glancing collision with dimethyl disulfide as a thermal electron donor (Scheme 2).[19] Because the electron transfer must occur over the distance of a few molecular diameters (5−10 Å),[39] the time scale for the formation of **1** is limited to <8 fs. This implies that the radical is initially formed with the geometry of the precursor ion. Hence, ion $\mathbf{1}^+$ must be prepared by a reliable method and its structure must be examined carefully by available experimental and computational methods.[14]

SCHEME 2

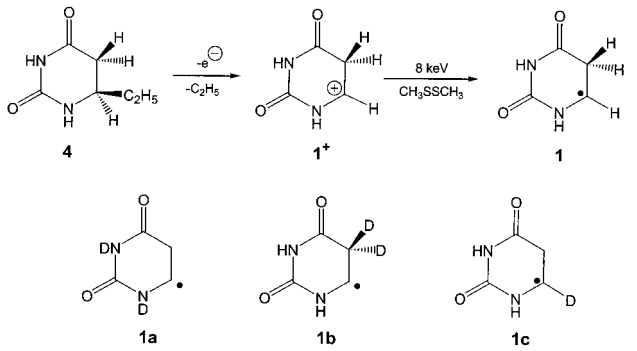

TABLE 1: Collisionally Activated Dissociation Spectra of Ions 1^+ and $1a^+-1c^+$

	relative intensity[a]					relative intensity[a]			
m/z	1^+	$1a^+$	$1b^+$	$1c^+$	*m/z*	1^+	$1a^+$	$1b^+$	$1c^+$
114		0.9	0.6		45	0.9	5.7	0.3	
113				0.7	44	1.4	4.4	5.3	3.0
112	1.1			0.2	43	5.7	5.0	4.8	4.8
97				0.2	41	3.3	3.3	2.2	2.9
87			0.6		40	3.0	1.9	1.0	1.5
86				0.2	39	1.0	0.7	0.5	0.6
85	0.7			0.5	38	0.7	0.7	0.8	0.6
84	0.5			0.2	30		0.5		0.2
72		0.9	61.5[b]	0.5	29	0.5	5.6	1.7	4.4
71	0.7	59.2[b]	1.6	64.4[b]	28	3.8	1.5	4.9	1.4
70	65.6[b]	4.0	2.7	4.0	27	1.0	1.0	1.3	0.8
69	3.8	1.8	0.8	0.4	26	0.7	0.8	0.5	0.4
68	1.6			0.9	17			0.8	
67	0.4			0.2	16			0.6	0.5
57				0.3	15	0.7	0.5		0.4
56	0.4				14				0.3
55	0.4								
54	0.4			0.3					
53	0.5			0.3					
52	0.5								

[a] Relative to the sum of CAD ion intensities. [b] Dominant product of metastable ion dissociations.

Ion Structures and Energetics. Cation 1^+ was generated efficiently by 70 eV dissociative ionization of 6-ethyl-5,6-dihydrouracil (**4**, Scheme 2). Deuterium-labeled ions $1a^+-1c^+$ were prepared accordingly using the labeled precursors **4a**−**4c**. Ion 1^+ showed a singlet peak in a high-resolution mass spectrum that had the correct elemental composition, $C_4H_5N_2O_2$ (measured 113.0348, calc. 113.0351), as established by accurate mass measurements. Ion 1^+ was further characterized by collisionally activated dissociation (CAD) mass spectra.

Unimolecular dissociations of 1^+ proceeded mainly by elimination of HNCO to form a $C_3H_4NO^+$ ion at *m/z* 70 (measured 70.0295, calculated 70.0293) that dominated the metastable-ion and CAD spectra (Table 1). Deuterium labeling in $1a^+-1c^+$ indicated a clean elimination of HNCO containing the N-1 and/or N-3 nitrogens that was not accompanied by hydrogen atom exchange between the N−H and C−H hydrogen atoms (Table 1). Energy calculations confirmed that elimination of HN═C═O containing C-2 and N-3 was the lowest-energy dissociation of 1^+ that required 165 kJ mol^{-1} to form HN═CH−CH_2−CO^+ (9^+) at the 0 K thermochemical threshold (Table 2). Formation of the isomeric CH_2═CH−NH−CO^+ (10^+) ion by elimination of HN═C═O containing C-4 and N-3 was slightly more endothermic and required 186 kJ mol^{-1} at the 0 K thermochemical threshold. These ring-cleavage dissociations may have activation energies above the dissociation thresholds (see below for radical dissociations), but these were not studied here. Loss of H atom from 1^+ to form the uracil cation-radical ($11^{+\bullet}$) was calculated to be substantially endothermic (360 kJ mol^{-1}, Table 2). The high threshold energy for the loss of H explained why it did not occur competitively in metastable-ion or collisionally activated dissociations.

Because electron ionization usually does not form ions with a narrow distribution of internal energies, a more specific ionization means was sought to generate 1^+. The appearance energy for the formation of 1^+ from **4** was calculated by B3−PMP2/6-311+G(2d,p). Assuming that **4** was thermalized at the ion source temperature (523 K), the calculated appearance energies (*AE*) ranged between 9.3 and 10.1 eV for the products ($1^+ + C_2H_5^\bullet$) formed with internal energies corresponding to 0 and 523 K, respectively. Charge-transfer ionization with $COS^{+\bullet}$ (IE = 11.18 eV)[40] was therefore deemed to be sufficiently exothermic to promote fast dissociation of $4^{+\bullet}$ to form 1^+ that would have a range of internal energies that was bracketed by the ionization exothermicity, IE(COS) − AE(1^+) = 1.08−1.88 eV and the lowest dissociation threshold of the ion (vide supra). In addition, the excess internal energy in the 1^+ thus formed (<1.9 eV) should be dissipated by collisions with COS in the high-pressure CI source. Fully thermalized 1^+ was calculated to have 43 kJ mol^{-1} mean internal energy at 523 K.

The relative energies of 1^+ and several other ion isomers were calculated at a high level of theory recently.[41,42] In the context of the present work, we note that 1^+ is only the fifth most stable isomer in the family of protonated uracil cations and is 82 kJ mol^{-1} less stable than N-1 protonated 2,4-dihydroxypyrimidine, which is the most stable ion isomer.[41,42] Regarding the other relevant ion isomers, it is noteworthy that cation 2^+ was unstable

TABLE 2: Ion Dissociation Energies

		energy[a]				
species/reaction	basis set	B3LYP	MP2[b]	B3-MP2[b]	QCISD[c]	QCISD(T)[c]
$1^+ \rightarrow 9^+$ + HN═C═O	6-31+G(d,p)	169				
	6-311+G(2d,p)	159	164	161	169	166
	6-311+G(2df,p)	158	164	161	169	166
	6-311+G(3df,2p)	156	163	159	169	165
$1^+ \rightarrow 10^+$ + HN═C═O	6-31+G(d,p)	191				
	6-311+G(2d,p)	169	177	173	187	183
	6-311+G(2df,p)	163	178	170	188	184
	6-311+G(3df,2p)	161	179	170	189	186
$1^+ \rightarrow 11^{+\bullet}$ + $H^\bullet$	6-31+G(d,p)	351				
	6-311+G(2d,p)	348	351 (359)[d]	349 (353)[d]	358 (358)[d]	356 (356)[d]
	6-311+G(2df,p)	346	350 (357)	348 (352)	357 (356)	355 (355)
	6-311+G(3df,2p)	347	355 (362)	351 (354)	361 (361)	360 (361)

[a] In units of kJ mol^{-1} at 0 K. [b] From spin-projected MP2 energies wherever it applies. [c] From effective energies with basis sets expanded according to eq 1. [d] From restricted open-shell MP2 calculations.

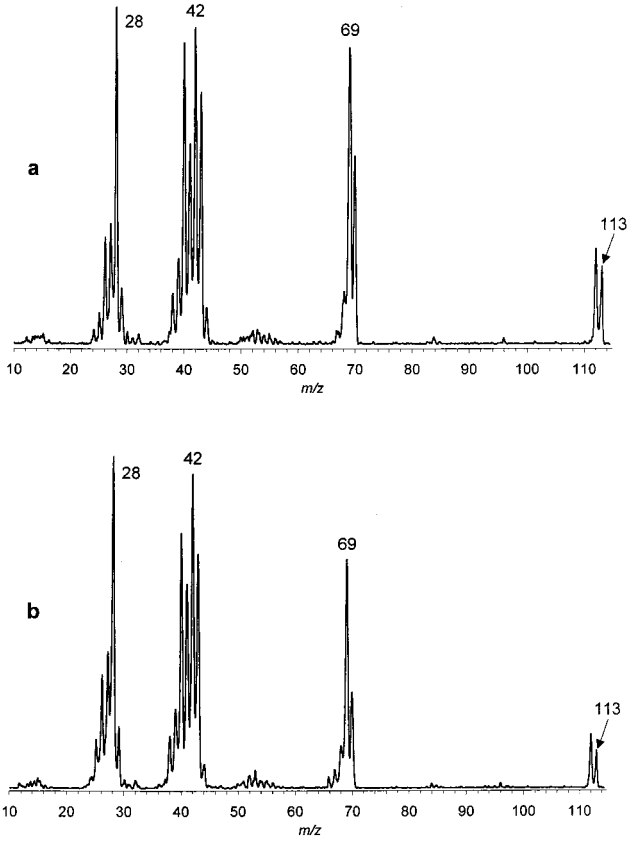

Figure 1. (a) Neutralization (CH_3SSCH_3, 70% transmittance)-reionization (O_2, 70% transmittance) mass spectrum of $\mathbf{1}^+$. (b) Neutralization (CH_3SSCH_3, 70% transmittance)-collisional activation (He, 50% transmittance)- reionization (O_2, 70% transmittance) mass spectrum of $\mathbf{1}^+$.

and isomerized spontaneously to $\mathbf{1}^+$.[41] It can be readily shown that an isomerization of $\mathbf{1}^+$ by intramolecular proton migration to form a more stable cation isomer must involve at least one four-membered transition state and therefore is likely to face a substantial energy barrier.[41] Ion $\mathbf{1}^+$ is therefore kinetically well stabilized against isomerization to more stable structures.

Formation and Dissociations of Radical 1. Collisional neutralization of $\mathbf{1}^+$ yielded a fraction of nondissociating radicals that following reionization gave rise to abundant survivor ions that appeared at *m*/*z* 113 in the NR mass spectrum (Figure 1a). The dissociations observed upon NR comprised loss of H (*m*/*z* 112) and ring-cleavages producing HNCO (*m*/*z* 43) together with the complementary C_3H_4NO fragment at *m*/*z* 70, C_3H_3NO at *m*/*z* 69, fragments of the C_2H_xN and CH_xN groups at *m*/*z* 38−42 and *m*/*z* 26−28, respectively, and CO at *m*/*z* 28.

The NR spectrum of $\mathbf{1}^+$ generated by charge exchange ionization with $COS^{+\bullet}$ of **4** was closely similar to the spectrum of the ion made by 70 eV electron ionization and is not shown separately. This indicated that effects on NR dissociations of $\mathbf{1}^+$ of the precursor ion energy were negligible or that stable $\mathbf{1}^+$ produced by electron ionization had internal energies close to thermal. Collisional activation with helium of the intermediate fast neutral species resulted in deeper dissociations that enhanced the formation of small fragments in the NCR spectrum (Figure 1b).

The dissociation mechanisms were elucidated by deuterium labeling. NR of the 1,3-D_2-labeled ion $\mathbf{1a}^+$ showed a clean (>95%) loss of a light hydrogen from C-5 and/or C-6 (Figure 2a). These positions were distinguished in the 6-D-labeled ion $\mathbf{1c}^+$ which upon NR showed clean (>99%) loss of a light hydrogen (Figure 2b). NR of the 5,5-D_2-labeled ion $\mathbf{1b}^+$ showed

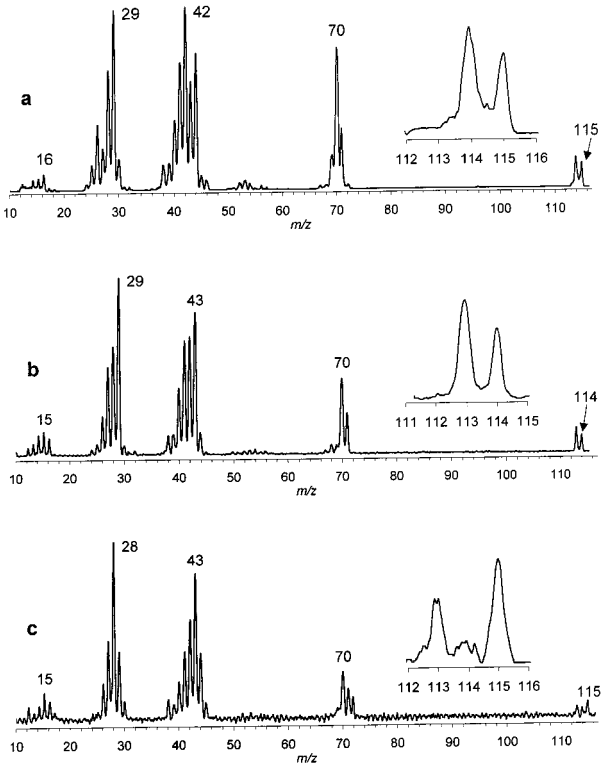

Figure 2. Neutralization (CH_3SSCH_3, 70% transmittance)-reionization (O_2, 70% transmittance) mass spectra of (a) $\mathbf{1a}^+$, (b) $\mathbf{1c}^+$, (c) $\mathbf{1b}^+$. The insets show expanded regions of survivor ion peaks from separate multiscan measurements.

predominant loss of D (Figure 2c), in line with the foregoing results. A small fraction of loss of H (ca. 15%) from $\mathbf{1b}^+$ can be attributed to an admixture of 1,5-D_2 or 3,5-D_2 isotopomers that were not distinguished by mass from $\mathbf{1b}^+$. The corresponding radicals were expected to eliminate H-5 rather than D-5, because of isotope effects (see below). The specific loss of H from the C-5 methylene group in **1** indicated exclusive formation of the most stable uracil tautomer **11** by NR dissociations.

The ring cleavage yielding C_3H_4NO showed predominant retention of H-1 and/or H-3 in the eliminated HNCO molecule, as evidenced by the appropriate mass shifts of *m*/*z* 70 to *m*/*z* 71 in the complementary $C_3(H,D)_4NO$ fragments (Figures 2a-2c). The HNCO molecule lost can include the C-2 carbonyl group in combination with the N-1-H or N-3-H groups, or the C-4 carbonyl and the N-3-H group. These were not distinguished by the present labeling experiments. Energy arguments favor cleavage of the C-4—C-5 and C-2—N-3 bonds to eliminate HNCO containing N-3 and C-4, as discussed below. Deuterium labeling further revealed that the *m*/*z* 28 fragment consisted of CO and HNCH, where the latter contained the C-6 methine group.

Dissociation Products of 1. To characterize some of the important fragments produced by dissociation of **1** we obtained reference NR spectra of the uracil cation radical ($\mathbf{11}^{+\bullet}$, *m*/*z* 112), $C_3H_4NO^+$ (*m*/*z* 70) prepared by dissociative ionization of **4**, and $C_3H_3NO^{+\bullet}$ (*m*/*z* 69) that was prepared from two different precursors, e.g., by dissociative ionization of uracil and maleimide by loss of HNCO and CO, respectively. The NR spectra are shown in Figure 3a−d. NR of uracil showed an abundant survivor ion in keeping with the stability of the neutral molecule (Figure 3a). The major dissociation was loss of HNCO to form C_3H_3NO at *m*/*z* 69. This is also an abundant dissociation of cation-radical $\mathbf{11}^{+\bullet}$ upon electron ionization and its occurrence

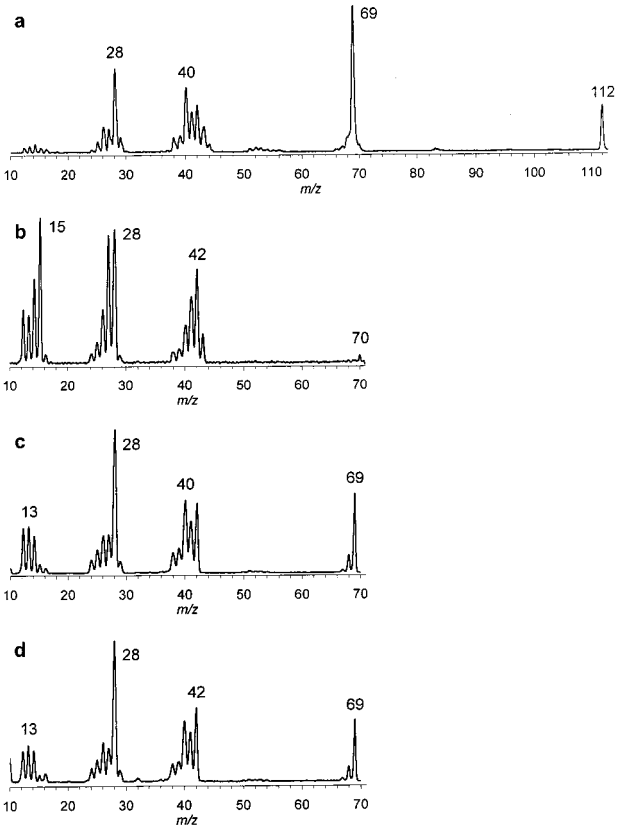

Figure 3. Neutralization (CH_3SSCH_3, 70% transmittance)-reionization (O_2, 70% transmittance) mass spectra of dissociation products: (a) $[uracil]^{+\bullet}$, (b) *m*/*z* 70 ion from dissociative ionization of **4**, (c) *m*/*z* 69 ion from dissociative ionization of uracil, and (d) *m*/*z* 69 ion from dissociative ionization of maleimide.

in the NR spectrum of $\mathbf{11}^{+\bullet}$ can be due to a combination of neutral and post-reionization dissociations. Interestingly, NR of $\mathbf{1}^+$ and $\mathbf{11}^{+\bullet}$ showed very similar [*m*/*z* 69]/[*m*/*z* 112] abundance ratios, 0.32 and 0.31, respectively, which indicated that the formation of the *m*/*z* 69 fragment from **1** was due to consecutive dissociations $\mathbf{1} \rightarrow \mathbf{11} \rightarrow C_3H_3NO^{+\bullet}$. In addition, one can use the relative abundances of *m*/*z* 112, *m*/*z* 69, and other ions in the NR spectrum of $\mathbf{11}^{+\bullet}$ to subtract the contributions of dissociations of reionized $\mathbf{11}^{+\bullet}$ in the NR spectrum of **1**.[43] These amounted to 45% of the total NR ion intensities and corresponded to the fraction of **1** that dissociated by loss of H-5 to form **11**. The remaining 55% of the NR fragment ion intensities were due to ring cleavage dissociations of **1** or post-reionization dissociations of $\mathbf{1}^+$. The contributions of the latter two processes were roughly estimated as follows. Assuming that the relative intensity of the *m*/*z* 70 ion in the NR spectrum (12.5%) was due entirely to dissociations of reionized $\mathbf{1}^+$ (see below), we obtain from the corresponding CAD relative intensity of the *m*/*z* 70 ion (60%) that $12.5/0.6 \approx 21\%$ of all ring fragments originated from reionized $\mathbf{1}^+$.[43] The contribution of the radical ring-cleavage dissociations was therefore $55-21 = 34\%$. After this separation of ion and radical dissociations, the branching ratio for ring cleavages and loss of H-5 in neutral **1** is estimated as $34/45 \approx 0.75$.

The NR spectra of the $C_3H_3NO^{+\bullet}$ ions prepared by dissociative ionization of uracil and maleimide were very similar and indicated identical ion structures or mixtures thereof (Figure 3c-d). The substantial survivor ion at *m*/*z* 69 indicated that the C_3H_3NO intermediate was a stable species. This indicates that if formed as a neutral molecule by dissociations of radical **1**, C_3H_3NO would be detected efficiently in the NR mass spectrum. We did not investigate the structure of the $C_3H_3NO^{+\bullet}$ fragment further, although the NR dissociations were compatible with both the $HN{=}CH{-}CH{=}C{=}O^{+\bullet}$ and 3-propenelactam$^{+\bullet}$ structures.

In contrast to C_3H_3NO, the NR spectrum of $C_3H_4NO^+$ (*m*/*z* 70) showed only a weak survivor ion and a dominant formation of CO (*m*/*z* 28) and $CH_2{=}CH{-}NH$ (*m*/*z* 42) (Figure 3b). This attested to the low stability of the C_3H_4NO radical in keeping with the calculated bond dissociation energy for $CH_2{=}CH{-}NH{-}C{=}O^{\bullet} \rightarrow CH_2{-}CH{=}NH^{\bullet} + CO$ that required only 7 kJ mol^{-1} at the 0 K threshold. The radical energetics is discussed in more detail later in the paper. The low stability of neutral C_3H_4NO corroborates the conclusion that the prominent *m*/*z* 70 peak in the NR spectrum of **1** must be due to a stable ion formed by a post-reionization dissociation of $\mathbf{1}^+$. Conversely, however, *transient formation* of $CH_2{=}CH{-}NH{-}C{=}O^{\bullet}$ from **1** followed by its *consecutive dissociations* is compatible with the formation upon NR of abundant low-mass fragments HNCO, $CH_2{-}CH{=}NH^{\bullet}$, and CO.

In summarizing the observed unimolecular dissociations of **1**, loss of a hydrogen atom from C-5 was a specific dissociation of the radical. Ring cleavages also occurred in **1** and gave rise to small-mass fragments HNCO, $CH_2{-}CH{=}NH$, and CO.

Dissociation Energetics of 1. To interpret the observed dissociations of uracil radicals, we performed ab initio and density functional calculations of the pertinent relative, activation, and dissociation energies. The energies were obtained at several levels of theory as summarized in Table 3. The energies obtained at the highest levels of theory, which in this work were effective QCISD(T)/6-311+G(3df,2p) and B3−PMP2/6-311+G(3df,2p), are visualized in a potential energy diagram (Figure 4). At all levels of theory **1** was the most stable uracil radical, followed by 5,6-dihydropyrimidine-2,4(*1H*,*3H*)-dion-5-yl (**2**), **3**, 4,5-dihydro-2-hydroxy-pyrimidine-4(*3H*)-on-2-yl (**12**, Figure 5), and 2-hydroxy-5,6-dihydropyrimidine-4(*3H*)-on-5-yl.[12] A number of other tautomeric radical structures were also calculated to be local energy minima, which are not discussed here. Out of these, radicals **1**, **2**, and **3** were hydrogen atom adducts to the most stable uracil tautomer **11**, which were of most interest for uracil radical chemistry.

The optimized structure of **1** was unexceptional, as shown in Figure 5. The ring in **1** was only slightly puckered with C-5 being out of plane and the axial hydrogen atom (H-5a) pointing nearly perpendicular to the ring. The radical site in **1** was localized mainly at C-6, as indicated by the calculated atomic spin density (0.92). The unpaired electron can activate cleavage of bonds to the adjacent atoms, e.g., N-1—C-2, N-1—H-1, C-5—H-5, and C-4—C-5. Dissociation products resulting from cleavage of these bonds were therefore of interest. Loss of H-5a was the lowest-energy dissociation of **1** that required 114 kJ mol^{-1} at the 0 K thermochemical threshold (Figure 4, Table 3). The dissociation involved a transition state (**TS1**) that was 133 kJ mol^{-1} above **1** and 19 kJ mol^{-1} above the products. Hence, addition of a H atom to C-5 in uracil had an activation energy barrier. Dissociation of the N-1—H-1 bond in **1** was 177 kJ mol^{-1} endothermic to form the less stable uracil tautomer **13**.[41,42] In addition, the dissociation must proceed through a transition state (**TS2**) that was 203 kJ mol^{-1} above **1** and 26 kJ mol^{-1} above the threshold energy for the formation of **13** and H atom. The large energy difference between **TS2** and **TS1** strongly favors elimination of H-5a in perfect agreement with experiment. A transition state (**TS3**) was also located for the 1,2-migration of a hydrogen atom from C-5 to C-6 that resulted in a mildly

TABLE 3: Dissociation and Activation Energies for Uracil Radicals 1 and 2

	energy[a,b]														
	reaction[c]														
method	(1)	(2)	(3)	(4)	(5)	(6)	(7)	(8)	(9)	(10)	(11)	(12)	(13)	(14)	(15)
B3LYP/6-31+G(d,p)	133	140	203	214	163	111	148	124	156	148	184	209	208	125	137
B3LYP/6-311+G(2d,p)	127	137	196	210	162	107	144	121	154	130	165	200	197	118	133
	126[d]	130												119	
B3LYP/6-311+G(2df,p)	125	135	198	211	161					128	168			116	131
B3LYP/6-311+G(3df,2p)	125	135	198	212	161	105	143	124	156	126	166	198	200	116	131
PMP2/6-311+G(2d,p)	100	124	165	199	165	117	151	120	154	148	170	222	209	89	119
	102[d]	124												93	
ROMP2/6-311+G(2d,p)	96	120	161	194	160	116	154	119	152	147	168	219	212	84	117
	98[c]	127												87	
PMP2/6-311+G(2df,p)	96	119	166	201	161					155	184			84	114
ROMP2/6-311+G(2df,p)	92	115	162	195	155					153	182			79	112
PMP2/6-311+G(3df,2p)	101	122	172	204	161	120	156	130	162	155	183	229	227	88	117
ROMP2/6-311+G(3df,2p)	97	118	168	199	155	119	158	129	161	154	181	226	231	83	115
QCISD/6-311+G(2d,p)															
PMP2	122	144	178	208	179	117	157	115	151	153	170	236	176	112	141
	123[d]	145													
ROMP2	122	145	179	210	178	119	156	116	152	154	167	235	177	112	141
	123[d]	144													
QCISD/6-311+G(2df,p)															
PMP2	117	140	180	210	174					159	183			107	136
ROMP2	118	140	180	211	173					160	184			107	137
QCISD/6-311+G(3df,2p)															
PMP2	122	142	185	213	174	120	161	124	159	160	182	243	195	111	139
ROMP2	123	143	186	215	173	121	160	125	161	161	183	242	196	112	139
QCISD(T)/6-311+G(2d,p)															
PMP2	113	134	170	199	173	114	150	112	144	147	165	220	179	102	130
ROMP2	114	135	170	200	171	115	149	113	146	148	165	219	179	102	131
QCISD(T)/6-311+G(2df,p)															
PMP2	109	130	172	200	168					154	179			97	126
ROMP2	109	131	172	202	166					155	179			97	126
QCISD(T)/6-311+G(3df,2p)															
PMP2	114	133	177	203	168	116	154	121	153	154	178	227	197	101	128
ROMP2	114	133	178	205	166	118	153	122	154	155	178	226	198	102	129
B3−PMP2/6-311+G(2d,p)	114	130	180	205	164	112	148	120	154	139	168	211	203	103	126
	114[d]	127												106	
B3−PMP2/6-311+G(2df,p)	110	127	182	206	161					141	176			100	123
B3−PMP2/6-311+G(3df,2p)	113	129	185	208	161	112	149	127	159	140	175	213	213	102	124

[a] In units of kJ mol^{-1} at 0 K. [b] From single-point energies on B3LYP/6-31+G(d,p) optimized geometries including zero-point vibrational energy corrections. [c] Reaction 1: **1** → **11** + H•. Reaction 2: **1** → **TS1**. Reaction 3: **1** → **13** + H•. Reaction 4: **1** → **TS2**. Reaction 5: **1** → **TS3**. Reaction 6: **1** → **14a**. Reaction 7:**1** → **TS5**. Reaction 8: **1** → **16b**. Reaction 9: **1** → **TS6**. Reaction 10: **1** → **10** + HNCO. Reaction 11: **1** → **9** + HNCO. Reaction 12: **1** → **TS7**. Reaction 13: **1** → **17** + CO. Reaction 14: **2** → **11** + H•. Reaction 15: **2** → **TS4**. [d] From single-point energies on HF/6-31G(d,p) optimized geometries (HF/6-31+G(d,p) for transition states) and zero-point energy corrections.

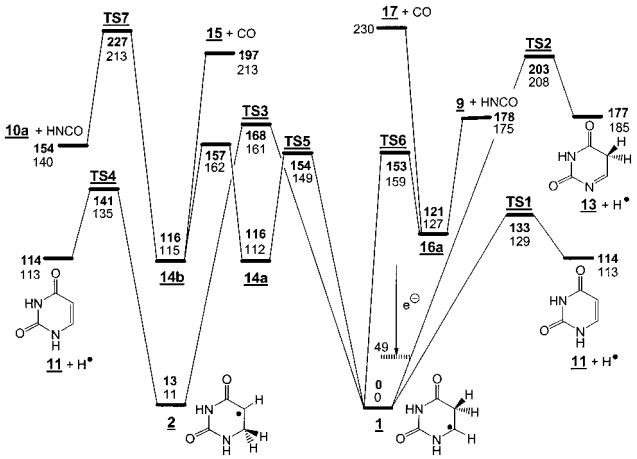

Figure 4. Potential energy diagram for dissociations of **1** and **2**. Roman numerals: B3−PMP2/6-311+G(3df,2p) energies. Bold numerals: Effective QCISD(T)/6-311+G(3df,2p) energies from basis set expansions through PMP2 calculations.

endothermic isomerization of **1** to **2**. However, the **TS3** energy (168 kJ mol^{-1} above **1**) was substantially higher than that for **TS1** (Table 3).

The large difference in the activation energies for the loss of H-5a and isomerization to **2** indicated that the former dissociation should be kinetically preferred. This was supported by RRKM calculations of unimolecular rate constants that were performed using both the effective QCISD(T)/6-311+G(3df,2p) and B3−PMP2/6-311+G(3df,2p) potential energy surfaces. In each case, the loss of H-5 was 2−3 orders of magnitude faster than the isomerization for reactant internal energies up to 200 kJ mol^{-1} above the threshold (Figure 6). Loss of a deuterium atom from C-5 in **1b** was also substantially faster than migration to C-6, as indicated by the pertinent RRKM rate constants (not shown). These findings were perfectly consistent with the results of deuterium labeling that showed a clean loss of a deuterium atom from C-5. Had isomerization to **2** occurred, H and D would have become equivalent at the C-6 methylene in the intermediate radical **2** and therefore would have been lost competitively. Interestingly, the transition state for the hydrogen atom loss from C-6 in **2** (**TS4**) was below **TS3**, so that loss of H-6 could also be expected to occur without isomerization to **1** (Figure 4).

Mechanisms for Ring Opening in 1. Ring cleavage dissociations of **1** were all endothermic (Figure 4). Dissociation of the C-4—C-5 bond proceeded with concomitant rotation of the incipient vinyl group about the N-1—C-6 bond to produce an open-ring intermediate, *anti-syn-syn-anti*-2,4-diazahex-5-en-1,3-dion-1-yl (**14a**, Scheme 3) that was 116 kJ mol^{-1} less stable than **1** (Table 3). This reaction path was confirmed by intrinsic reaction coordinate calculations[44] from the transition state for

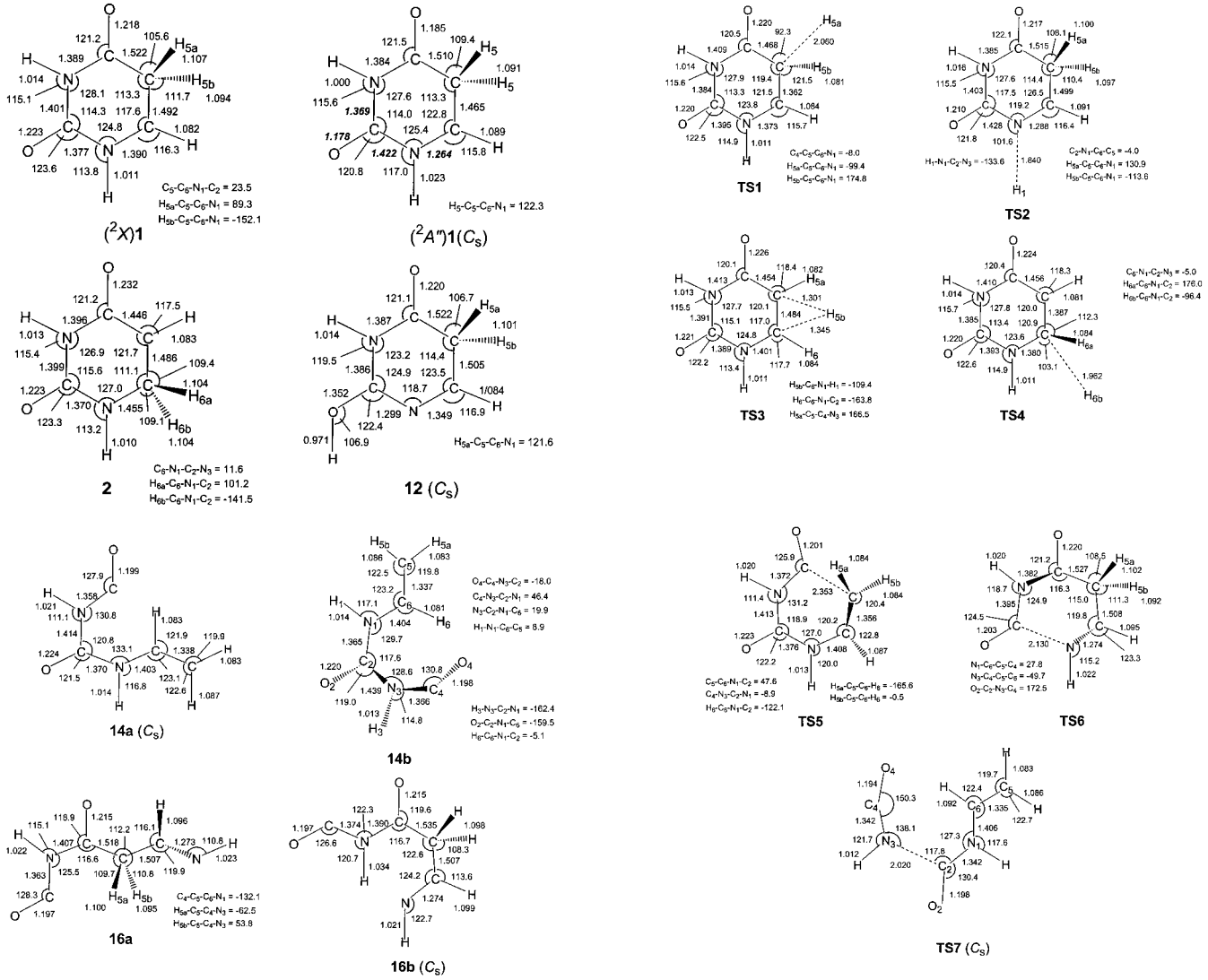

Figure 5. B3LYP/6-31+G(d,p) optimized structures of uracil radicals in ground electronic state. Bond lengths in ångstroms, bond and dihedral angles in degrees. The structure of the ^2A state of **1** was optimized with UCIS/6-31+G(d,p). The bond lengths in the ^2A state that differed most from those in the ^2X state are shown as bold italics.

the ring opening (**TS5**). Radical **14a** can isomerize by internal rotations to produce several other conformers (Scheme 3). Note that because there are four bonds for internal rotations in **14a**, e.g., N-3—C-4, C-2—N-3, N-1—C-2, and N-1—C-6, there are 16 theoretically possible combinations of conformers, of which the *anti-syn-syn-syn* conformer is identical with **1**, and the all-*syn* conformer is impossible for steric reasons. We calculated the relative energies of the *syn-syn-syn-anti* (**14b**), *anti-anti-syn-anti* (**14c**), *anti-anti-syn-syn* (**14d**), all-*anti* (**14e**), and *syn-syn-anti-anti* (**14f**) conformers, which all had at least one favorable alignment of the C—O and N—H bond dipoles. The 0 K enthalpies of the conformers relative to **14a** were −1, 2, 4, −6, and −31 kJ mol^{-1} for **14b**, **14c**, **14d**, **14e**, and **14f**, respectively.

Because the open-ring radicals **14a-14f** represent isomers of **1** and not detectable dissociation products, the energetics of their further dissociations were also investigated. A dissociation of the C-2—N-3 bond in **14a**−**d** and **14f** can produce *anti-anti*-CH_2═CH−NH−CO$^\bullet$ (**10a**) and HNCO that was calculated to require 154 kJ mol^{-1} from **1**. *syn-anti*-CH_2═CH−NH−CO$^\bullet$ (**10b**) was 9 kJ mol^{-1} less stable than the *anti-anti* conformer **10a**, so that the formation of **10b** had a correspondingly higher threshold energy. Dissociation of **1** via **14b** by loss of the C-4—O carbonyl to form the *anti-anti* conformer of the N-vinyl-N′-ureidyl radical, CH_2═CH−NH−CO−NH$^\bullet$ (**15**, Scheme 3), required 197 kJ mol^{-1} at the 0 K thermochemical threshold and was therefore substantially more endothermic than the loss of HNCO.

Another mechanism for ring cleavage in **1** comprised dissociation in **1** of the N-1—C-2 bond with concomitant rotation about the C-4—C-5 and C-5—C-6 bonds to produce an open-ring intermediate, *anti-anti-syn-anti*-1,5-diazahex-1-en-4,6-dion-6-yl (**16a**) (Scheme 4), that was 121 kJ mol^{-1} less stable than **1**. The (*Z*)-*syn-syn-anti-anti*-(**16b**) and all-*anti* (**16c**) conformers were also stable structures whose respective 0 K enthalpies were 1 and 20 kJ mol^{-1} relative to **16a**. A further dissociation of **16a** to HN═CH−CH_2−CO$^\bullet$ (**9**) and HNCO required 58 kJ mol^{-1} so that the product threshold energy was 178 kJ mol^{-1} above **1**. Dissociation of **1** via **16a** by loss of the C-2-O carbonyl to yield the *syn-anti* conformer of the 3-imidopropionamidyl radical (**17**, Scheme 4) was substantially endothermic and required 230 kJ mol^{-1} at the 0 K thermochemical threshold (Figure 4).

In addition to their inherent endothermicities, the ring cleavages in **1** involved additional activation barriers that were calculated as 154 (**TS5**) and 153 kJ mol^{-1} (**TS6**) for the cleavages of the C-4—C-5 and N-1—C-2 bonds, respectively (Figure 4). Hence, the activation energies for the ring cleavages

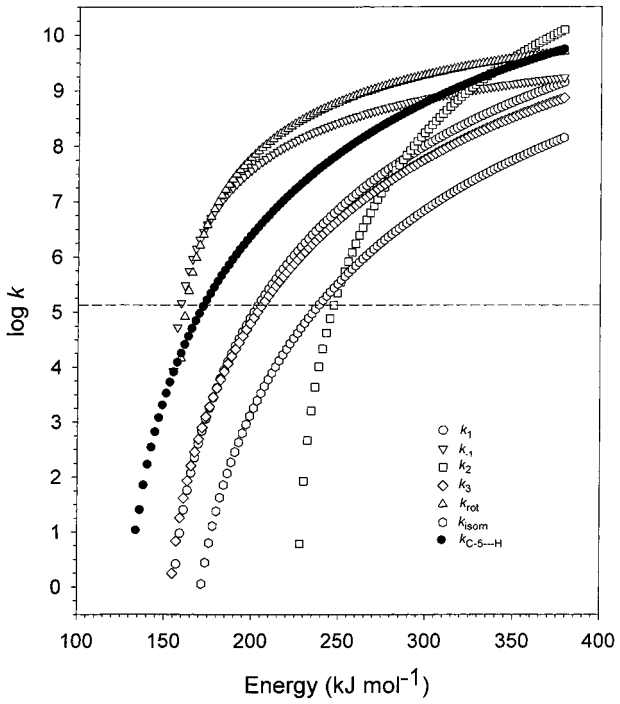

Figure 6. RRKM unimolecular rate constants for dissociations and isomerizations of **1**. Full circles: Dissociation of the C-5—H bond. Empty circles: Ring-opening by cleavage of C-4—C-5 bond (k_1). Upside-down triangles: Ring closure **14a** → **1** (k_{-1}). Squares: Dissociation **14a** → **10a** + HNCO (k_2). Diamonds: Ring-opening by cleavage of N-1—C-2 bond (k_3). Triangles: Rotation in **14a** → **14b**. Hexagons: Isomerization **1** → **3**. The dashed line at log $k = 5.13$ corresponds to the rate constant for 50% dissociation on the experimental time scale.

SCHEME 3

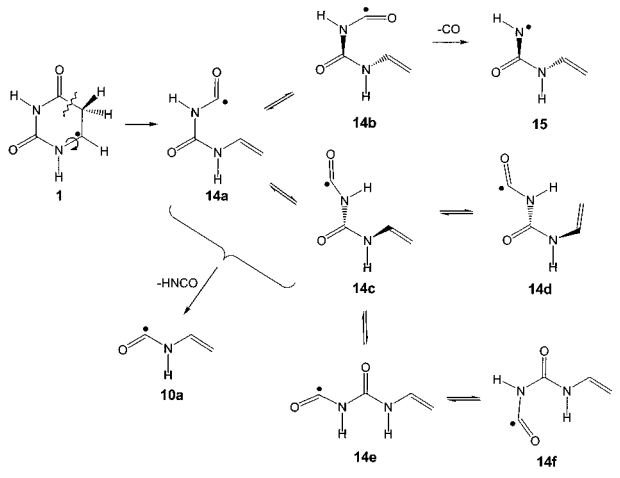

in **1** were greater than that for loss of H-5a, but comparable to that for isomerization to **3**.

Comparison of Radical Dissociation and Activation Energies Calculated at Different Levels of Theory. The data in Table 3 allowed us to compare the performance of the various schemes used to calculate the total of 15 dissociation and activation energies for uracil radicals. As benchmark values, we chose the effective QCISD(T)/6-311+G(3df,2p) energies with which the other energies, calculated at presumably lower levels of theory, were compared. The value of such comparisons is in identifying schemes that equal or approach the performance of the benchmark scheme, but are computationally less demanding and therefore practical for use with even larger open-shell systems.

SCHEME 4

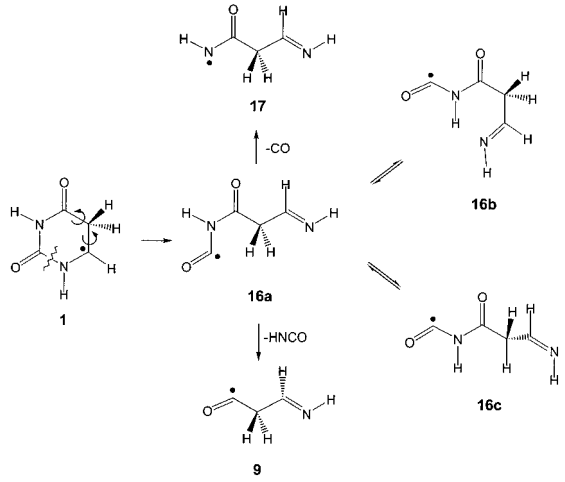

The data in Table 3 (reactions 1, 3, 11, 13, and 14) showed that B3LYP calculations mostly *overestimated* bond dissociation energies in uracil radicals for basis sets ranging from 6-31+G(d,p) through 6-311+G(3df,2p). In contrast, PMP2 calculations with these basis sets mostly *underestimated* bond dissociation energies. Simple averaging of the B3LYP and PMP2 energies (denoted B3—PMP2) thus often resulted in error cancellation and provided excellent agreement with the benchmark dissociation energies. In addition, the fit between the B3—PMP2 and benchmark energies showed only a weak dependence on the basis set used, so that even the relatively inexpensive[45] B3—PMP2/6-311+G(2d,p) dissociation energies were within 4 kJ mol^{-1} root-mean-square deviation of the benchmark data. Experimental data are scarce to provide a rigorous check for the calculated parameters. We note, however, that the calculated adiabatic ionization energy of uracil, 9.23 and 9.25 eV from B3—PMP2/6-311+G(2d,p) and effective QCISD(T)/6-311+G(3df,2p), respectively, (Table 4) reproduced very well the experimental IE_a (9.2 eV) that was extrapolated from the photoelectron spectrum.[46] Likewise, the B3—PMP2/6-311+G(2d,p) electron affinity of uracil (0.055 eV) compares well with the experimental values, 0.054 eV[47] and 0.093 eV.[48]

The transition state energies calculated with B3LYP/6-31+G(d,p) showed very good agreement with the benchmark energies (reactions 2, 4, 5, 7, 9, 12, and 15, Table 3). However, because B3LYP calculations overestimated bond dissociation energies, they severely underestimated the barriers for hydrogen atom additions, as noted previously for other systems.[49]

The B3—PMP2 transition state energies were mostly in very good agreement with the benchmark data. The largest deviation was for **TS7** (reaction 12, Table 3) which was underestimated by B3—PMP2 by 13—16 kJ mol^{-1}. However, the overall agreement with the benchmark energies, including reaction 12, was within 9 kJ mol^{-1} rmsd. We also note that effective QCISD calculations consistently overestimated bond dissociation and transition state energies by 9 kJ mol^{-1} rmsd. These deviations canceled out in the calculations of activation energies for hydrogen atom additions for which QCISD performed at the benchmark level. It may also be noted that relative energies from spin-projected MP2 calculations did not differ significantly from the ROMP2-based values in B3-MP2 or effective QCISD(T) calculations.

In summary, inexpensive B3—PMP2/6-311+G(2d,p) calculations provide very good estimates of bond dissociation and transition state energies in uracil radicals when compared with benchmark effective QCISD(T)/6-311+G(3df,2p) data. Other

TABLE 4: Ionization and Franck−Condon Energies

	ionization energy[a]		Franck−Condon energy	
method	**1**	**11**	**1**	
			VN[b]	VI[c]
B3LYP/6-31+G(d,p)	6.96	9.21		
B3LYP/6-311+G(2d,p)	6.92	9.21	46	62
B3LYP/6-311+G(2df,p)	6.93	9.22	45	
B3LYP/6-311+G(3df,2p)	6.92	9.22	45	63
PMP2/6-311+G(2d,p)	6.66	9.25	54	65
ROMP2/6-311+G(2d,p)	6.61	9.33	53	
PMP2/6-311+G(2df,p)	6.70	9.34	52	
ROMP2/6-311+G(2df,p)	6.66	9.41	52	
PMP2/6-311+G(3df,2p)	6.72	9.35	52	65
ROMP2/6-311+G(3df,2p)	6.68	9.43	52	
QCISD/6-311+G(2d,p)[d]	6.70	9.14		
QCISD/6-311+G(2df,p)[d]	6.74	9.23		
QCISD/6-311+G(3df,2p)[d]	6.77	9.24		
QCISD(T)/6-311+G(2d,p)[d]	6.63	9.14		
QCISD(T)/6-311+G(2df,p)[d]	6.68	9.23		
QCISD(T)/6-311+G(3df,2p)[d]	6.70	9.25		
B3−PMP2/6-311+G(2d,p)	6.79	9.23	50	64
B3−PMP2/6-311+G(2df,p)	6.81	9.28	49	
B3−PMP2/6-311+G(3df,2p)	6.82	9.28	49	64

[a] Adiabatic ionization energies at 0 K in electronvolts. [b] Energy difference in units of kJ mol^{-1} between the vertically neutralized radical and the optimized neutral structure. [c] Energy difference in units of kJ mol^{-1} between the single-point energy of the cation with the optimized radical structure and the energy of the optimized cation structure. [d] Effective energies from basis set expansions (eq 1).

schemes, e.g., B3LYP and effective QCISD, showed systematic bias in dissociation or transition state energy calculations.

Kinetics of Competing Dissociations of 1. The effective QCISD(T) and B3−PMP2 transition state energies were used in RRKM calculations of the unimolecular rate constants for loss of H-5a and ring cleavage dissociations in **1.** Figure 6 shows the RRKM rate constants based on the effective QCISD(T) energies; those based on the B3−PMP2 energies showed very similar trends and are not discussed separately. The dissociation to *anti-anti*-CH_2═CH−NH−CO$^{\bullet}$ (**10a**) and HNCO proceeds in a minimum of three steps, e.g., **1** ↔ **14a** → **14b** → **10a**, where the ring-opening is reversible. The rate of formation of **10a** is in general time-dependent,[50] but can be approximated by the time-independent Bodenstein (steady-state) formula[51] through an effective rate constant, $k_{eff} = k_1k_2/(k_{-1} + k_2)$, where k_1 is the rate constant for ring opening by C-4−C-5 bond dissociation in **1**, k_{-1} is the rate constant for the reverse ring closure, and k_2 is the rate constant for the dissociation of the open-ring intermediate **14a**. The branching ratio for the ring cleavage dissociation and loss of H-5a is given by k_{eff}/k_H, where k_H is the rate constant for the hydrogen atom loss. Exact evaluation of the $k_2/(k_{-1} + k_2)$ term to find the *kinetically most favorable* dissociation route would be a daunting task because of the multitude of conformers in the open-ring intermediates **14a**−**f**, rotational barriers for their interconversion (Figure 4), and the multitude of transition states for the loss of HNCO from the conformers. We have investigated the potential energy profiles for dissociations of the C-2−N-3 bonds in **14a**−**14f**, which all showed potential energy barriers above the dissociation threshold corresponding to the formation of **10a**. As a case in point, a transition state (**TS7**) was obtained for the loss of HNCO from **14b** that was 112 kJ mol^{-1} above **14b** and 227 kJ mol^{-1} above **1** (Figure 4). This was significantly higher than the barrier for intramolecular rotation about the CO−NH bond interconverting **14a** and **14b**, which was 41 kJ mol^{-1} above **14a**. According to RRKM calculations (Figure 6), the **14a** ↔ **14b** interconversion was faster than the loss of HNCO in open-ring intermediates **14a** and **14b** having up to 230 kJ mol^{-1} internal energy. Hence, except for a fraction of highly energetic radicals, the dissociation was the rate-determining step. RRKM calculations of the rate constants for the dissociation of **14b** (k_2) and ring closure in **14a** (k_{-1}) showed $k_2/(k_{-1} + k_2)$ values ranging between 0 and 0.94 for internal energies from **TS7** up to 260 kJ mol^{-1} above **14a** (379 kJ mol^{-1} above **1**). Note the crossover of the log k curves for k_2 and k_{-1} at $E = 323$ kJ mol^{-1} (Figure 6). Hence, the upper bound for the branching ratio for the ring cleavage dissociations vs loss of H is given simply by k_1/k_H. The calculated RRKM rate constants indicate that, at all levels of theory, $0 < k_1/k_H < 0.25$ for **1** having internal energies between that of the dissociation threshold and 380 kJ mol^{-1}. Hence, $k_{eff}/k_H < 0.25$ and the loss of H-5a *should predominate at all internal energies*.[52]

Discussion of Radical Dissociations: The Role of Excited Electronic States. The calculated potential energy surfaces suggested that elimination of a hydrogen atom should dominate the unimolecular dissociations of radical **1**. In the discussion we now compare the predicted dissociations with those observed for radicals generated by collisional electron transfer.

The NR dissociations of **1** showed specific loss of a hydrogen from C-5 that was not accompanied or preceded by isomerization to **2**. This was in keeping with the RRKM calculated rate constants for these competitive reactions that predicted the loss of H-5a to be substantially faster (Figure 6). Note that the absence of unimolecular isomerization **1** ↔ **2** in the gas phase contrasts the acid−base-catalyzed isomerization of uracil radicals in solution.[5] Referring back to the present gas-phase data, the calculated rate constants also indicated that ring cleavage dissociations should not compete efficiently with the loss of H-5a, which was in sharp contrast with NR dissociations of **1** in which ring-cleavage dissociations producing HN═C═O and CH_2CH═NH accounted for about 34% products.

Another question related to the NR dissociations concerned the internal energy in the radicals formed by collisional electron transfer that drives the observed dissociations. We have shown previously for related heterocyclic radicals[14a,14b] that the vibrational energy in the species that were formed in the *ground electronic state* was convoluted from the internal energy of the precursor cation and the Franck−Condon energy acquired upon vertical electron transfer. With **1**, the sum of the ion mean thermal energy, e.g., 43 kJ mol^{-1} for $\mathbf{1}^+$ generated by charge-exchange ionization followed thermalization at 523 K, and the Franck−Condon energy (Table 4) results in an estimated 43 + 49 = 92 kJ mol^{-1} mean vibrational energy in the radical.[14a] This is substantially less than the transition state energy for the lowest-energy dissociation (**TS1**, 133 kJ mol^{-1}, Table 3). In addition, the loss of H-5a showed ca. 37 kJ mol^{-1} kinetic shift to attain rate constants allowing 50% dissociation on the 5.1 μs time scale. The internal energy needed for a kinetically relevant loss of H-5a can possibly be accessed in a fraction of radicals belonging to the high-energy tail of the internal energy distribution curve. However, a dissociation by ring-cleavage, including the **TS5** energy and an associated 43 kJ mol^{-1} kinetic shift,[53] would require that dissociating **1** contain >190 kJ mol^{-1} internal energy, which can be accessed only by an extremely small fraction of the highest-energy radicals. Clearly, these cannot account for the ca. 34% of ring dissociations observed. The competition between the loss of hydrogen atom and ring cleavage dissociations is thus incompatible with the estimated internal energy distribution in radicals formed in the ground electronic state.

TABLE 5: Excited State Energies of Radical 1

radical optimized geometry	state	ΔE[a]		f[b]		$\tau(\mu s)$		configuration[c]	
		CIS[d]	TD-B3LYP[e]	CIS	TD-B3LYP	CIS	TD-B3LYP	CIS	TD-B3LYP
(*X*) 1[f]	A	5.26	3.21	0.002	0.010	0.4	0.2	30α → 31α	30α → 31α
	B	5.64	3.76	0.0004	0.0015	1.8	1.1	mixed α,β[h]	30α → 32α
	C	5.72	4.37	0.001	0.001	0.7	1.2	mixed α,*β*	29*β* → 30*β*
	D	6.03	4.51	0.011	0.007	0.06	0.2	mixed α,*β*	30α → 33α
	E	6.36	4.73	0.001	0.0003	0.6	3.4	mixed α,*β*	30α → 34α
(*A*) 1[i]	A	3.66	2.31	0.0014	0.012	1.2	0.4	30α → 31α	30α → 31α
	B	4.95	2.47	0.0001	0.001	9.4	3.8	mixed α[h]	30α → 32α
	C	5.04	3.40	0.031	0.000	0.03	>20	mixed α	30α → 33α
	D	5.08	3.63	0.001	0.0001	0.9	17.5	30α → 33α	30α → 34α
	E	5.42	4.01	0.010	0.005	0.08	0.3	mixed α	30α → 35α
1+[j]	A	3.84	2.02	0.0013	0.011	1.2	0.5	30α → 31α	30α → 31α
	B	5.00	2.60	0.031	0.0009	0.03	3.8	mixed α	30α → 32α
	C	5.03	3.42	0.000	0.0001	>20	20	mixed α	30α → 33α
	D	5.13	3.60	0.0007	0.000	1.25	>20	30α → 33α	30α → 34α
	E	5.38	3.94	0.0001	0.040	8.0	0.04	mixed α	30α → 35α

[a] Excitation energies in units of electronvolt. [b] Oscillator strengths. [c] Dominant configurations with expansion coefficients >0.85. [d] From spin unrestricted UCIS/6-311+G(2d,p) single-point calculations. [e] From time-dependent UB3LYP/6-311+G(2d,p) single-point calculations. [f] UB3LYP/6-31+G(d,p) optimized geometry of the ground electronic state. [g] From time-dependent UB3LYP/6-31+G(d,p) calculations. [h] Configurations consisting of several α and/or *β* electron excitations. [i] UCIS/6-31+G(d,p) optimized geometry of the excited *A* state. [j] B3LYP/6-31+G(d,p) optimized geometry of the cation.

It has been pointed out recently that excited electronic states play an important role in the dissociations of radicals formed by femtosecond collisional electron transfer.[14a,14b,54] This is due to the fact that the incoming electron can enter an unoccupied orbital in the cation or cause excitation of a valence electron to form the radical in an excited electronic state. Bright excited states that have short (<ns) radiative lifetimes compared to the *μ*s time scale for dissociations will emit a photon and decay to the ground electronic state without affecting the dissociation kinetics. In contrast, photochemically dark states that have *μ*s or longer radiative lifetimes can dissociate on the corresponding potential energy surfaces or undergo internal conversion through avoided crossings or conical intersections to a vibrationally excited lower electronic state. Such dark excited states can be expected to affect the dissociation kinetics by opening new dissociation channels or by funneling the electronic energy to vibrational energy of the ground electronic state.

Excited States of 1. We have addressed the energetics of excited electronic states in **1** by time-dependent density functional theory (TD-B3LYP) and configuration interaction singles (CIS) calculations. The former approach has been shown to provide reliable excitation energies for several molecular systems, whereas the energies from CIS calculations are typically overestimated and do not converge to the ionization limit.[15] CIS calculations, combined with gradient optimizations, were used to obtain geometries for local energy minima of the first excited state (^2A) that in turn served for single-point energy calculations with TD-B3LYP. The calculated energies, oscillator strengths, radiative lifetimes, and dominant configurations of the five lowest excited states of **1** are summarized in Table 5, and the ^2X, ^2A, and ^2B states depicted in Figure 7.

The ^2A through ^2E excited states formed by vertical neutralization of $\mathbf{1}^+$ all had energies that were above those for the transition states for the hydrogen losses or ring cleavages in ground state **1**. Hence, any of the radiationally long-lived excited states can drive the fragmentations of ground-state **1** following internal conversion. The calculated radiative lifetimes of the vertically formed ^2A through ^2E states, $\tau = 1/A_{ij}$, where A_{ij} is the Einstein coefficient for spontaneous radiative transition to the ground state, were in the *μ*s range, although it must be noted that the values calculated by CIS and TD-B3LYP differed (Table 5). Following vertical electron capture to form the excited state

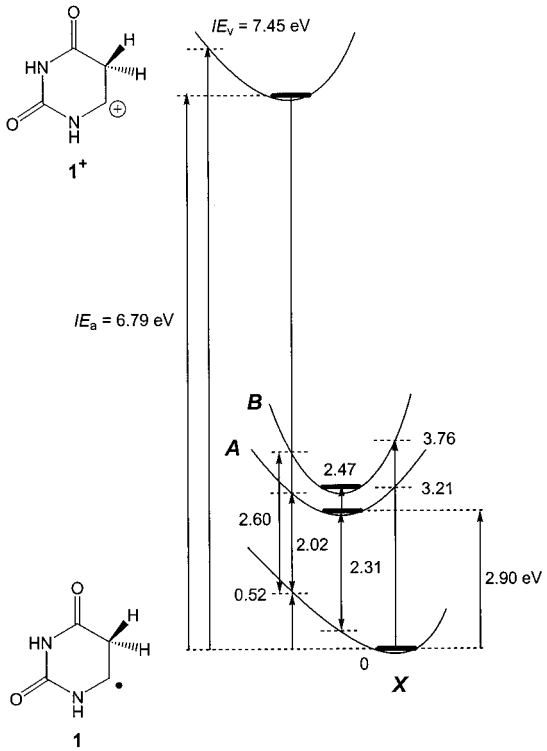

Figure 7. TD-B3LYP/6-311+G(2d,p) excitation and B3−PMP2/6-311+G(2d,p) ionization energies of **1**.

in a nonrelaxed geometry, the vibrational wave packet unfolds rapidly on the potential energy surface to distribute the internal energy among the vibrational degrees of freedom.[55] Because the Franck−Condon energies in vertical electron capture were low, e.g., 25 kJ mol^{-1} from the CIS energies of the vertically formed and fully optimized ^2A state, most of the vibrational modes must remain in $v = 0$ states.[56] Therefore, the radiative lifetime of radicals formed by electron capture in the ^2A state also depends on the transition moments from the geometry of the corresponding potential energy minimum. Table 5 shows that the radiative lifetime of the relaxed ^2A state was comparable to that formed by vertical electron capture, and a similar situation was expected for the higher excited states, as well.[57]

Can ring-cleavage dissociations occur on the excited-state potential energy surface? Although detailed investigation of excited-state potential energy surfaces of **1** would be a daunting task, an insight can be gained from the comparison of the optimized geometries of the ^2X and ^2A states of **1** (Figure 5). Compared with the ^2X state, the ^2A state had a planar ring (C_s symmetry) and showed a substantial elongation of the N-1—C-2 bond and concomitant shortening of the N-1—C-6, C-2—N-3, and C-2—O-2 bonds. These changes upon electron excitation are consistent with the weakening of the N-1—C-2 bond to facilitate ring cleavage.

Conclusions

The hydrogen atom adduct to the C-5 in uracil was generated specifically in the gas phase and found to be stable on the 5.1 μs time scale. The dissociations of uracil radicals generated by femtosecond electron capture are driven by the formation of excited electronic states. Specific loss of an axial hydrogen from the C-5 methylene in radical **1** was observed in accord with the calculated transition state energies and RRKM dissociation rate constants. In addition, abundant ring-cleavage dissociations occurred in the radicals that resulted in expulsion of HNCO and CO.

Acknowledgment. Support of this work by NSF (Grants Nos. CHE-9712570 and CHE-0090930) is gratefully acknowledged. Computational facilities used in this work were supported by NSF (Grant No. CHE-9808182) and the University of Washington. Thanks are due to Dr. Martin Sadilek for assistance with CAD spectra measurements.

References and Notes

(1) von Sonntag, C. In *Physical and Chemical Mechanism in Molecular Radiation Biology*; Glass, W. A., Varma, M. N., Eds.; Plenum Press: New York, 1991; pp 287−321.

(2) Steenken, S. *Chem. Rev.* **1989**, *89*, 503.

(3) Flossmann, W.; Westhof, E.; Müller, A. *J. Chem. Phys.* **1976**, *64*, 1688.

(4) Westhof, E.; Lion, Y.; van de Vorst, A. *Int. J. Radiat. Biol.* **1977**, *32*, 499.

(5) Deeble, D. J.; Das, S.; von Sonntag, C. *J. Phys. Chem.* **1985**, *89*, 5784.

(6) Pullman, B.; Pullman, A. *Quantum Biochemistry*; Interscience Publishers: New York, 1963.

(7) (a) Hayon, E.; Simic, M. *J. Am. Chem. Soc.* **1973**, *95*, 1029. (b) Fujita, S.; Steenken, S. *J. Am. Chem. Soc.* **1981**, *103*, 2540.

(8) (a) Symons, M. C. R. *J. Chem. Soc., Faraday Trans. 1* **1987**, *83*, 1. (b) Candeias, L. P.; Steenken, S. *J. Phys. Chem.* **1992**, *96*, 937.

(9) (a) Hayon, E. *J. Chem. Phys.* **1969**, *51*, 4881. (b) Myers, L. S.; Hollis, M. L.; Theard, L. M.; Peterson, F. C.; Warnick, A. *J. Am. Chem. Soc.* **1970**, *92*, 2875.

(10) (a) Henriksen, T.; Snipes, W. *J. Chem. Phys.* **1970**, *52*, 1997. (b) Box, H. C.; Budzinski, E. E. *J. Chem. Phys.* **1975**, *62*, 197. (c) Sagstuen, E.; Hole, E. O.; Nelson, W. H.; Close, D. M. *J. Phys. Chem.* **1989**, *93*, 5974. (d) Ohta, N.; Tanaka, N.; Ito, S. *J. Chem. Soc., Perkin Trans. 2* **1999**, 2597.

(11) (a) Krauss, M.; Osman, R. *J. Phys. Chem.* **1993**, *97*, 13515. (b) Colson, A.-O.; Sevilla, M. D. *J. Phys. Chem.* **1995**, *99*, 13033. (c) Colson, A.-O.; Sevilla. M. D. *Int. J. Radiat. Biol.* **1995**, *67*, 627. (d) Colson, A.-O.; Becker, D.; Eliezer, I.; Sevilla, M. D. *J. Phys. Chem. A* **1997**, *101*, 8935.

(12) Wolken, J. K.; Syrstad, E. A.; Vivekananda, S.; Turecek, F. *J. Am. Chem. Soc.* **2001**, *123*, 5804.

(13) For most recent reviews, see: (a) Zagorevskii, D. V.; Holmes, J. L. *Mass Spectrom. Rev.* **1999**, *18*, 87. (b) Schalley, C. A.; Hornung, G.; Schroder, D.; Schwarz, H. *Chem. Soc. Rev.* **1998**, *27*, 91.

(14) For applications of NRMS to the gas-phase chemistry of heterocyclic radicals see: (a) Wolken, J. K.; Turecek, F. *J. Am. Chem. Soc.* **1999**, *121*, 6010. (b) Wolken, J. K.; Turecek, F. *J. Phys. Chem. A*, **1999**, *103*, 6268. (c) Nguyen, V. Q.; Turecek, F. *J. Am. Chem. Soc.* **1997**, *119*, 2280. (d) Nguyen, V. Q.; Turecek, F. *J. Mass Spectrom.* **1997**, *32*, 55. (e) Nguyen, V. Q.; Turecek, F. *J. Mass Spectrom.* **1996**, *31*, 1173. (f) Turecek, F. *J. Mass Spectrom.* **1998**, *33*, 779.

(15) Stratmann, R. E.; Scuseria, G. E.; Frisch, M. J. *J. Chem. Phys.* **1998**, *109*, 8218.

(16) Wolken, J. K.; Turecek, F. *J. Phys. Chem. A* **2001**, *105*, 8352.

(17) Lee, C. K.; Shim, J. Y. *Bull. Korean Chem. Soc.* **1991**, *12*, 343.

(18) Turecek, F.; Gu, M.; Shaffer, S. A. *J. Am. Soc. Mass Spectrom.* **1992**, *3*, 493.

(19) Turecek, F. *Org. Mass Spectrom.* **1992**, *27*, 1087.

(20) Frisch, M. J.; Trucks, G. W.; Schlegel, H. B.; Scuseria, G. E.; Robb, M. A.; Cheeseman, J. R.; Zakrzewski, V. G.; Montgomery, J. A., Jr.; Stratmann, R. E.; Burant, J. C.; Dapprich, S.; Millam, J. M.; Daniels, A. D.; Kudin, K. N.; Strain, M. C.; Farkas, O.; Tomasi, J.; Barone, V.; Cossi, M.; Cammi, R.; Mennucci, B.; Pomelli, C.; Adamo, C.; Clifford, S.; Ochterski, J.;. Petersson, G. A.; Ayala, P. Y.; Cui, Q.; Morokuma, K.; Malick, D. K.; Rabuck, A. D.; Raghavachari, K.; Foresman, J. B.; Cioslowski, J.; Ortiz, J. V.; Stefanov, B. B.; Liu, G.; Liashenko, A.; Piskorz, P.; Komaromi, I.; Gomperts, R.; Martin, R. L.; Fox, D. J.; Keith, T.; Al-Laham, M. A.; Peng, C. Y.; Nanayakkara, A.; Gonzalez, C.; Challacombe, M.; Gill, P. M. W.; Johnson, B. G.; Chen, W.; Wong, M. W.; Andres, J. L.; Head-Gordon, M.; Replogle, E. S.; Pople, J. A. *Gaussian 98, Revision A.6*, Gaussian, Inc., Pittsburgh, PA, 1998.

(21) (a) Becke, A. D. *J. Chem. Phys.* **1993**, *98*, 1372, 5648. (b) Stephens, P. J.; Devlin, F. J.; Chabalowski, C. F.; Frisch, M. J. *J. Phys. Chem.* **1994**, *98*, 11 623.

(22) Rauhut, G.; Pulay, P. *J. Phys. Chem.* **1995**, *99*, 3093.

(23) (a) Finley, J. W.; Stephens, P. J. *J. Mol. Struct. (THEOCHEM)* **1995**, *357*, 225. (b) Wong, M. W. *Chem. Phys. Lett.* **1996**, *256*, 391. (c) Scott, A. P.; Radom, L. *J. Phys. Chem.* **1996**, *100*, 16 502.

(24) Møller, C.; Plesset, M. S. *Phys. Rev.* **1934**, *46*, 618.

(25) (a) Schlegel, H. B. *J. Chem. Phys.* **1986**, *84*, 4530. (b) Mayer, I. *Adv. Quantum Chem.* **1980**, *12*, 189.

(26) McWeeny, R.; Diercksen, G. *J. Chem. Phys.* **1968**, *49*, 4852.

(27) Parkinson, C. J.; Mayer, P. M.; Radom, L. *J. Chem. Soc.* Perkin Trans. 2 **1999**, 2305.

(28) Turecek, F. *J. Phys. Chem. A* **1998**, *102*, 4703.

(29) (a) Turecek, F.; Wolken, J. K. *J. Phys. Chem. A* **1999**, *103*, 1905. (b) Turecek, F.; Carpenter, F. H. *J. Chem. Soc. Perkin Trans. 2* **1999**, 2315. (c) Turecek, F.; Polasek, M.; Frank, A. J.; Sadilek, M.: *J. Am. Chem. Soc.* **2000**, *122*, 2361.

(30) Rablen, P. R. *J. Am. Chem. Soc.* **2000**, *122*, 357.

(31) Pople, J. A.; Head-Gordon, M.; Raghavachari, K. *J. Chem. Phys.* **1987**, *87*, 5968.

(32) Curtiss, L. A.; Raghavachari, K.; Pople, J. A. *J. Chem. Phys.* **1993**, *98*, 1293.

(33) (a) Curtiss, L. A.; Redfern, P. C.; Smith, B. J.; Radom, L. *J. Chem. Phys.* **1996**, *104*, 5148. (b) Smith, B. J.; Radom, L. *J. Phys. Chem.* **1995**, *99*, 6468.

(34) Foresman, J. B.; Head-Gordon, M.; Pople, J. A.; Frisch, M. J. *J. Phys. Chem.* **1992**, *96*, 135.

(35) Zhu, L.; Hase, W. L. *Quantum Chemistry Program Exchange*; Indiana University: Bloomington, Indiana, 1994. Program No. QCPE 644.

(36) Frank, A. J.; Sadilek, M.; Ferrier, J. G.; Turecek, F. *J. Am. Chem. Soc.* **1997**, *119*, 12 343.

(37) Zhu, L.; Hase, W. L. *Chem. Phys. Lett.* **1990**, *175*, 117.

(38) Levine, I. N. *Physical Chemistry*, 3rd ed.; McGraw-Hill: New York, 1988; p 839.

(39) Holmes, J. L. *Mass Spectrom. Rev.* **1989**, *8*, 513.

(40) *NIST Standard Reference Database No. 69*, February 2000 Release. http://webbook.nist.gov/chemistry.

(41) Wolken, J. K.; Turecek, F. *J. Am. Soc. Mass Spectrom.* **2000**, *11*, 1065.

(42) Podolyan, Y.; Gorb, L.; Leszczynski, J. *J. Phys. Chem. A* **2000**, *104*, 7346.

(43) The relative intensities in the CAD spectra obtained at kiloelectronvolt collision energies are insensitive to the internal energy of the ion, see for example: Busch, K. L.; Glish, G. L.; McLuckey, S. A. *Mass Spectrometry/Mass Spectrometry*, VCH Publishers: New York, 1988; pp 163−166. With uracil ions and $\mathbf{1}^+$, decreasing the precursor ion transmittance from 70% (17% multiple collisions) to 50% (31% multiple collisions) changed the fragment ion relative intensities by <5%.

(44) Gonzalez, C.; Schlegel, H. B. *J. Phys. Chem.* **1990**, *94*, 5523.

(45) Typical CPU running times on IBM RS/6000 for B3LYP and MP2/6-311+G(2d, p) single point calculations were under 3 h, as compared to QCISD(T)/6-31G(d, p) calculations that took 36 h and required over 7 GB scratch disk space.

(46) Yu, C.; O'Donnell, T. J.; LeBreton, P. R. *J. Phys. Chem.* **1981**, *85*, 3851.

(47) Desfrancois, C.; Abdoul-Carime, H.; Schermann, J. P. *J. Chem. Phys.* **1996**, *104*, 7792.

(48) Hendricks, J. H.; Lyapustina, S. A.; de Clercq, H. L.; Snodgrass, J. T.; Bowen, K. H. *J. Chem. Phys.* **1996**, *104*, 7788.

(49) (a) Nguyen, M. T.; Creve, S.; Vanquickenborne, L. G. *J. Phys. Chem.* **1996**, *100*, 18 422. (b) Jursic, B. S. *Chem. Phys. Lett.* **1996**, *256*,

603. (c) Skokov, S.; Wheeler, R. A. *Chem. Phys. Lett.* **1997**, *271*, 251. (d) Basch, H.; Hoz, S. *J. Phys. Chem. A* **1997**, *101*, 4416.

(50) Connors, K. A. *Chemical Kinetics*, VCH Publishers: New York, 1990; p 101.

(51) Bodenstein, M. *Z. Physik. Chem.* **1913**, *85*, 329.

(52) Time-dependent branching ratios were also calculated for dissociation times $t = 1/k_H$ and showed values between 0 and 0.20 for internal energies in **1** ranging from **TS7** to 360 kJ mol^{-1}.

(53) Lifshitz, C. *Mass Spectrom. Rev.* **1982**, *1*, 309.

(54) (a) Polasek, M.; Turecek, F. *J. Am. Chem. Soc.* **2000**, *122*, 9511. (b) Frank, A. J.; Turecek, F. *J. Phys. Chem. A* **1999**, *103*, 5348. (c) Nguyen, V. Q.; Sadilek, M.; Frank, A. J.; Ferrier, J. G.; Turecek, F. *J. Phys. Chem. A* **1997**, *101*, 3789.

(55) See for example: Lehmann, K. K.; Pate, B. H.; Scoles, G. In *Mode Selective Chemistry*; Jortner, J., Levine, R. D., Pullman, B. Eds.; Kluwer: Dordrecht, 1991; pp 17−23.

(56) Dunbar, R. C. *J. Chem. Phys.* **1989**, *90*, 7369.

(57) This follows from the fact that as the electron is promoted to higher excited states and becomes less tightly bound, the excited-state geometry of the radical resembles more closely that of the ion. Hence, Franck−Condon effects on vertical electron capture diminish when higher excited states of the radical are formed.